Hindawi
Journal of Nanotechnology
Volume 2024, Article ID 7426184, 17 pages
https://doi.org/10.1155/2024/7426184

Research Article

Tunable High-Frequency Acoustoelectric Current Oscillations in Fluorine-Doped Single-Walled Carbon Nanotubes

Daniel Sekyi-Arthur,[1] **Samuel Yeboah Mensah**,[2] **Kofi Wi-Adu**,[3] **Kwadwo Anokye Dompreh**,[2] **and Raymond Edziah**[2]

[1]*Department of Physics, College of Basic and Applied Sciences, University of Ghana, PMB, Accra, Ghana*
[2]*Department of Physics, College of Agriculture and Natural Sciences, University of Cape Coast, PMB, Cape Coast, Ghana*
[3]*Material Research Institute, The Pennsylvania State University, University Park, State College, Pennsylvania 16802, USA*

Correspondence should be addressed to Daniel Sekyi-Arthur; rasdean3@gmail.com

Received 27 October 2023; Revised 12 December 2023; Accepted 12 February 2024; Published 25 March 2024

Academic Editor: Valery Khabashesku

Herein, we report on a fluorine-doped single-walled carbon nanotube (FSWCNT) phenomenon, that yields tunable high-frequency self-sustained acoustoelectric direct current (ADC) oscillations. A tractable analytical method was used in the hypersound domain, to base the calculations on carriers in the lowest miniband. Hypothetically, the energy of interaction between the carriers and the acoustic phonons is less than the energy of the typical carriers. High-order harmonics of the acoustic phonons' effective field could be disregarded under this supposition. The ADC was observed to exhibit a nonlinearity, that resulted from the carrier distribution function's distortion as a result of interaction with the acoustic phonons, which had strong nonlinear effects. Theoretically, we demonstrated that the dynamics of space charge instabilities, due to Bragg reflection of Bloch oscillating carriers in the FSWCNT's miniband, were the only factors which contributed to the creation of radiation in the terahertz (THz) frequency range. The study also investigated the influence of various FSWCNT parameters such as the overlapping integrals (Δ_s and Δ_z), ac-field (E_1), and carrier concentration (n_o)on the behaviour of the ADC. The results showed that the intensity of the ADC oscillation (J_{zz}^{ae}/J_o^{ae}) could be tuned by adjusting Δ_s, Δ_z, E_1, and n_o.This tunability suggests that FSWCNTs could be used as an active device operating at very high frequencies, potentially reaching the submillimeter wavelength range. The study also suggests the possibility of domain suppression and acoustic Bloch gain through dynamic ADC stabilisation.

1. Introduction

Terahertz (THz) radiation indeed has a myriad of applications in various fields, specifically science and industry. The THz region of the electromagnetic (EM) spectrum, located between the microwave and infrared frequencies with wavelength $1mm$ to about $100\mu m$ (i.e. frequency range of 300 GHz to 3 THz), offers unique opportunities for studying molecular resonances and interactions [1]. In other to create a functional coherent THz radiation source or amplifier at ambient temperature, researchers have explored different approaches. Employing superlattices (SLs) and the nonlinear interaction of high-frequency electric field with miniband carriers in dc-biased SLs is one intriguing technique. This idea expands on past research by Ktitorov et al. [1] and Esaki-Tsu [2]. In this system, miniband carrier Bloch oscillations can potentially lead to the amplification of THz radiation [3]. Bloch oscillations, which refer to the periodic motion of carriers in the crystalline lattice being influenced by a static electric field, are a fundamental quantum phenomenon. By carefully designing the SL structure and applying static electric field, it is possible to exploit this effect and generate THz radiation [1, 2].

Buttiker et al. demonstrated the phenomenon of negative differential velocity (NDV) caused by Bragg scattering in a semiconductor [4]. They demonstrated this effect over decades ago, showing that NDV can lead to the propagation of electric field domains in a semiconductor and the

generation of self-sustained current oscillations without the need for an external resonator [4–7]. The phenomenon of self-sustaining current oscillations in an SL has been experimentally observed by Le Person et al. [8–10]. They utilised picosecond light pulses to generate and observe photocurrent oscillations in an SL, which decayed over time. Furthermore, reports in [11] indicate the observance of self-sustaining current oscillations up to a frequency of 20 MHz in a doped GaAs/AlAs SL. These oscillations were achieved under voltage control at a temperature of 5 K, specifically in the region of sequential tunneling where Bragg-reflected carriers are unlikely to be detected.

However, despite achieving this milestone, there are still some challenges associated with realising these THz amplifiers. One significant obstacle is the development of high-field electric domains inside the SL [9, 12–25]. These electric domains are necessary for achieving NDC, which is crucial for the amplification process [9, 12]. Overcoming these challenges and realising practical, ambient temperature THz amplifiers are an active area of research. Advances in semiconductor technology, device fabrication techniques, and understanding of quantum phenomena are contributing to the progress in this field. Successful development of compact and efficient THz radiation sources and amplifiers can have significant implications for a wide range of applications, including communications, spectroscopy, imaging, and sensing.

A single-walled carbon nanotube (SWCNT), a novel material with an exceptional carrier conductivity and inherent nonlinearity due to their one-dimensional structure, makes SWCNT a potential for RF (radio frequency) electronic application [26–28]. SWCNT-based RF transistors have shown impressive transport characteristics and density of states, leading to advancements in the field over the last decade. SWCNT-FETs (SWCNT-field-effect transistors) have achieved significant milestones in terms of their intrinsic maximum oscillation frequency ($f_{T,\mathrm{int}}$) and maximum frequency ($f_{\max,\mathrm{int}}$). For instance, certain SWCNT-FETs have demonstrated $f_{T,\mathrm{int}}$ values as high as 153 GHz, while other SWCNT-FETs have attained $f_{\max,\mathrm{int}}$ values as high as 70 GHz. These accomplishments have cleared the path for the creation of analog radio systems and high-speed circuits based on SWCNT-FETs [29–33]. In addition to this, SWCNT film-based radio-frequency transistors (SWCNTFBRFTs) have been reported to exhibit maximal hypersound oscillation frequencies exceeding 100 GHz [29–33].

The unique skeletal structure of SWCNTs allows for the attachment of foreign atoms to the surface without compromising the tubular structure. Doping SWCNTs with atoms such as fluorine can transform an armchair-SWCNT from a metallic state to a semiconducting state [34–39]. Doping increases carrier concentration and expands the bandstructure's existing states, further modifying the material's behaviour [34–41]. The exceptional properties of SWCNTs, such as their carrier conductivity, nonlinearity, and ability to be doped, have propelled advancements in SWCNT-based RF electronics, including the development of high-speed circuits and analog radio systems. These advancements have the potential to revolutionize the field of RF technology [30–33].

As to why we chose fluorine-doped SWCNTs to elements like Cl, Br, and I was due to FSWCNT's semiconducting properties. Taborowska et al. conducted investigation into the doping of SWCNTs with halogenated solvents (i.e., dichloromethane, chloroform, and bromoform) [34]. They found out that using halogenated solvents as the medium significantly enhances the carrier conductivity at room temperature. For SWCNT, films made in an acetone/toluene mixture had a carrier conductivity of $853 \pm 62\, Scm^{-1}$ [35], but when dichloromethane and chloroform were used, the carrier conductivity increased to $1652 \pm 186\, Scm^{-1}$ and $1966 \pm 425\, Scm^{-1}$, respectively. The Br-SWCNT specimen created in bromoform shows an even more noticeable rise. The Br-SWCNT's carrier conductivity increases were quadrupled in comparison to the material made utilising nonhalogen solvents, reaching $3819 \pm 241\, Scm^{-1}$. The measured values were quite high despite the mild chemical nature of these molecules [36].

The carrier conductivity, which reduces as temperature rises, indicated that the SWCNT networks were basically metallic in nature [36]. Due to this, the Seebeck coefficient values of variously produced SWCNT films were adequate but not outstanding. The doped-SWCNT room temperature Seebeck coefficient of $46 \pm 3\mu V/K$ matched the performance of other undoped SWCNT-based thermogenerators [37]. In contrast, the Seebeck coefficients for the ensembles made in dichloromethane (SWCNT/DCM), chloroform (SWCNT/CF), and bromoform (SWCNT/BF) were 26 ± 2, 22 ± 3, and $19 \pm 1\mu V/K$, respectively. Therefore, the observed drop in Seebeck coefficients strongly suggests that the material was doped when processed using these halogenated aromatic solvents on a regular basis. Doping changed the material from nondegenerate to degenerate character, which had a significant impact on the carrier conductivity but a detrimental impact on the thermoelectric power [38]. Doping also increased the carrier concentration and added more state to the already existing band structure. The increase in carrier conductivities brought on by doping was responsible for the decline in Seebeck coefficients.

Although changing chirality can also yield a semiconducting tube as doping, doping with fluorine is a quick, easier, fast, and more economical way to enhance the carrier density and also modify the carrier band structure from metallic to semiconducting p-type FSWCNT. Such an internal chirality is inherent and included during the band structure derivation of carbon nanotubes [2, 3]. The one-dimensional semiconducting FSWCNT benefits from the ADC effect because a "high-frequency-induced phase-dependent dc current by Bloch oscillator nonohmicity" using an external field has been observed by Seeger et al. in a 3-dimensional superlattice (SL) [39], Seidu et al. in a quasi-one dimensional SWCNT [40], and Mensah et al. in a nonparabolic semiconductor [41]. Moreover, due to the high nonparabolicity and carrier density of FSWCNT, the dc generated was much higher than in the other materials.

In this study, we focus on calculating the high-frequency ADC of FSWCNTs in the presence of acoustic phonons.

The characteristics under investigation, such as the ADC and carrier momenta, are significantly influenced by various factors, including the geometric chiral angle (GCA, θ_h), temperature (T), and real overlapping integrals for jumps along the tubular axis (Δ_z) and base helix (Δ_s). FSWCNTs are being explored as potential candidates for THz applications, and their ADC generation becomes particularly interesting when these parameters undergo variation. However, it is worth noting that prior to this study, no research had been conducted on the high-frequency ADC oscillations of FSWCNTs to the best of our knowledge. Therefore, the primary goal of this study was to investigate and analyse the high-frequency ADC oscillations in FSWCNTs. Understanding the acoustoelectric response of FSWCNTs can contribute to the development of novel technologies by utilising these materials in the THz frequency range.

2. Theory

To solve the problem in the semiclassical regime, the following conditions were utilised:

(i) $\Delta_{s,z} \gg \tau^{-1}$ ($\hbar = 1$): This condition implies that the energy gap between the spin-up and spin-down states, denoted by $\Delta_{s,z}$, is larger than the inverse of the scattering time τ. It suggests that scattering processes between the spin states are negligible compared to the energy difference.

(ii) $\omega \gg 1/\tau$: This condition states that the frequency of the electric field ω should be much larger than the inverse scattering time $1/\tau$, indicating that the system responds quickly to the external field.

(iii) $\omega_q \ll \vartheta(p)$: This condition assumes that the characteristic phonon frequency ω_q is much smaller than the energy ($\vartheta(p)$) of the carriers. In other words, the energy carried by the carriers dominates over the energy associated with phonons.

(iv) $\omega \gg \Delta_{s,z}$: The frequency of the external electric field should be much larger than the energy gap between the spin states. It ensures that the energy provided by the electric field is sufficient to drive transitions between the spin states.

(v) Carriers are available only in the lowest miniband, and interminiband transitions are neglected: This assumption implies that the carriers (i.e. electrons or holes) are confined to the lowest energy miniband in the FSWCNT. Transitions between different minibands are disregarded, simplifying the problem by focusing only on the behaviour of carriers within the lowest miniband.

(vi) The carrier gas is nondegenerate: This condition suggests that the carrier gas is in a nondegenerate state, meaning that the distribution of carriers follows classical statistics rather than quantum statistics. It allows for the use of classical approaches in analysing the FSWCNT's carrier behaviour.

(vii) The phonons, which represent the lattice vibrations, are in a state of thermal equilibrium. This implies the distribution of phonons follows a thermal distribution corresponding to the temperature of the FSWCNT.

(viii) For a frequency range of 100 GHz to 3 THz and a nanotube of 100 nm at a high temperature $> r\text{bin } 50K$ (or 5 meV), low-temperature quantum effects such as Coulomb blockade become irrelevant: Under this condition, the frequency range and size of the system, along with the temperature, are such that quantum effects like Coulomb blockade can be ignored. In other words, the classical approximation is valid under these conditions.

(ix) Wave phenomena such as reflection and tunneling are negligible in the hypersound regime ($q\ell \gg 1$ and $\omega\tau \gg 1$). In this regime, high-frequency acoustic phonons can be treated as particles with energy (and momentum), allowing for a semiclassical treatment. The absence of reflections is explained by approximating the slowly varying potential as a large number of small potentials. The small reflections at each interface interfere destructively, resulting in no net reflection. The carriers (phonons in this case) can then be described semiclassically, following Newton's laws.

(x) If the energy gained by the carrier from the external field is much smaller than the overlapping integral (the energy scale associated with the slowly varying potential, $\Delta_{s,z}$) along the characteristic length ($d_{s,z}$) of the system, and the scattering rate (ν) is small compared to the energy picked up by the carrier from the electric field, then the carrier will oscillate within the first miniband with Bloch frequency ($\omega_B = eEd_{s,z}/\hbar$). The carrier's energy and group velocity become periodic functions of time. In this scenario, the semiclassical approximation ($i.e. \Delta_{s,z} \gg eEd_{s,z}$) is satisfied, allowing for the carrier to be treated semiclassically using classical equations of motion.

(xi) Under the semiclassical condition, the carrier wave packet, representing the carrier, is treated as a particle. The uncertainty in the electron's momentum is assumed to be minimal, making the carrier's energy sharply defined. In addition, the uncertainty in the carrier's position is considered to be minimal compared to the spatial variations of the applied and built-in potentials. The motion of the center of the wave packet is described by the equation $\hbar k/dt = -\nabla\vartheta = F$, which resembles the classical relation between force and momentum.

(xii) The relaxation time (τ) is the characteristic time it takes for a system to return to its equilibrium state after being perturbed. In doped SWCNTs, the relaxation time is much smaller than that of undoped SWCNTs. This suggests that doped

SWCNTs exhibit faster relaxation dynamics. The wavelength of the wave is denoted as $= 2\pi/q$ ($\ell = 10^{-6}cm$), which is much less than that of the carrier free path length ($\lambda = 10^{-6}cm$). In this context, the condition $q\ell \gg 1$ is satisfied which implies that the wave's characteristic length scale is much smaller than the average distance a carrier can travel without scattering.

We consider a single longitudinal acoustic wave that travels along a uniform FSWCNT tube that has electrical insulation at both ends. In order to guarantee that there is no wave reflection at the termination, the travelling acoustic wave is created by driving one end of the tube with a vibrator or interdigital transducer (IDT 1) and matching the other end to an appropriate acoustic impedance (IDT 2). Because the tube's ends are electrically isolated, the acoustic wave would pull carriers to one end, leaving the other end lacking in carriers. The conventional electric current produced by the resulting electric field along the tube precisely cancels out the current related to the acoustoelectric effect. Therefore, by measuring the electric potential difference between the tube's tyro ends, the acoustoelectric effect may be quantified. Surprisingly, this process is similar to how temperature differences cause voltage to be generated in an open circuit during the thermoelectric effect. One way to think of the net flow of travelling acoustic waves over a temperature gradient is as a net flow of phonons.

The acoustoelectric current density is determined as follows [42–45]:

$$J = \frac{e\Phi\Lambda^2 q^2 \tau}{(2\pi\hbar)^2 \rho v_s \omega_q} \sum_p \int_0^\infty [F(p) - F(p+q)][v(p+q) - v(p)] \times \delta\left(\vartheta_{p+q} - \vartheta_p - \omega_q\right) d^2 p, \tag{1}$$

where Φ, Λ, ρ, v_s, and ω_q are the acoustic phonon flux density, deformation potential constant, FSWCNT's density, velocity of sound, and frequency of the acoustic waves, respectively. As a result, we describe the FSWCNT's energy dispersion relation as in [46–50]:

$$\vartheta(p) = \vartheta_o - \Delta_s \cos\left(\frac{p_s d_s}{\hbar}\right) - \Delta_z \cos\left(\frac{p_z d_z}{\hbar}\right), \tag{2}$$

where $d_s = \sqrt{3}b_s/2$, $d_z = 3\sqrt{3}b_z/2$, and $b_{s,z}$ is the $c - c$ bond length along the base helix and tubular directions, respectively. The Δ_s and Δ_z (supposed for clarity to be real) are the overlap integrals for transitions along the spiral (base helix) and between the coils (tubular). The quantities (Δ_s and Δ_z) are phenomenological adjustable parameters to be determined for a real SWCNT by first-principle numerical calculations; their estimates are given in [51].

We adhere to the proposition of Romanov and Kibis' phenomenological spiral (helicoidal) model [51–53]. Let us consider a system of atoms arranged periodically with $b_{s,z}$ intervals along the spiral line, which twines at an angle θ_h round a circular cylinder of radius $R \gg b_{s,z}$ and contains $N \gg 1$ atoms per coil. For the sake of simplicity, we assume the nearest atoms of neighbouring coils to be situated ($b_{s,z} = 2\pi R \tan\theta_h$) just at the same element of the cylinder (i.e., $2\pi R/b_{s,z} \cos\theta_h$ integer and equal to N). The true honeycomb crystalline structure of graphene is ignored in favour of treating FSWCNTs as a periodic chain of carbon atoms strung together on a helix. By taking into account a periodic structure of coaxial atomic rings, with the same distance between atoms in each ring as between two nearby rings, the spiral model simplifies the analysis. This approach allows for analytical calculations and provides insights into the properties of doped nanotubes like FSWCNTs and BC2N. It is noteworthy that the spiral model is specifically applicable to doped nanotubes, such as FSWCNTs and BC2N, rather than pure carbon nanotubes [53–55].

FSWCNT exhibits a two-scale periodicity as a result of its chiral geometry: one scale is caused by the helical pitch and the other by the interatomic lengths along the base helix. The carrier momenta p_s and p_z are along the base helix and tubular axis, respectively. b_s is the distance between the site n and $n+1$ along the base helix, and b_z is the distance between the site n and $n+N$ along the tubular axis. Due to the transverse quantisation of carrier motion not being taken into account before, both p_s and p_z change arbitrarily within the first Brillouin zone [55]. Here, we emphasise that the overall equality between N jumps along the base helix and one hop along the tubular axis is not guaranteed. The carrier velocities at the ending sites are different for the two leaps despite the fact that both jumps begin at the same site (l) with the same initial velocity and conclude at the same site ($N + l$). The carrier velocity has a circumferential component for travel along the base helix but not for motion along the tubular axis. This demonstrates that an FSWCNT is totally a quantum structure and that the classical minimal action principle cannot be used since quantum theory permits multiple ways for atoms to connect together. By doing this, we ignore the interference between the axial and helical paths that connect two atoms and consider the $\mathscr{Z}-$ and $\mathscr{S}-$ components of momentum to be independent of one another. Actually, this indicates that transverse motion quantisation is not something we take into account [53–55].

The carrier miniband velocity along the $\mathscr{S}$ and $\mathscr{Z}$ coordinates was calculated using (2) as $v = \partial\vartheta(p)/\partial p$ [46, 47, 50];

$$v_s(p_s) = \frac{\Delta_s d_s}{\hbar} \sin\left(\frac{p_s d_s}{\hbar}\right), v_z(p_z) = \frac{\Delta_z d_z}{\hbar} \sin\left(\frac{p_z d_z}{\hbar}\right). \tag{3}$$

The Boltzmann transport equation for carriers interacting with an acoustic wave of frequency (ω_q) and wavenumber (q) in the presence of a high-frequency electric field was quoted as

$$\frac{\partial F(r,p,t)}{\partial t} + v \cdot \frac{\partial F(r,p,t)}{\partial r} + e\left[\mathscr{E}_o + \mathscr{E}_1 \cos(\omega t)\right] \frac{\partial F(r,p,t)}{\partial p} = \left(\frac{\partial F}{\partial t}\right)_{\text{col}}, \tag{4}$$

where $F(r, p, t)$ represents the nonequilibrium carrier distribution function, $v(p)$ represents the carrier miniband velocity, p represents the carrier quasi-momentum, and τ represents the carrier relaxation time. The LHS of (4) results from a change in the distribution function due to time dependence, spatial gradients, and external forces, whereas the RHS arises from a change in the distribution due to the collision processes.

The preceding approach is semiclassical, wherein the carriers are treated as classical particles, except for their adherence to quantum principles (Fermi–Dirac). The initial requirement for this semiclassical approach to be applicable is that the wavelength of phonons needs to be significantly greater than the de Broglie wavelength of the particles, i.e., $\lambda_{ph} \gg \lambda_{el}$. If this scenario holds true, the movement of the carrier can be approached in a classical manner, except for their statistics. By doing this, it becomes possible to treat the ions as a spread-out continuous positive background, rather than needing to consider the lattice's discrete nature. This preceding condition is also crucial if we plan to take into account the effects of lattice deformation through a deformation potential.

The equation describing the motion of the carriers in FSWCNT when subjected to a high-frequency external electric field, along with the given initial conditions $t' = t$ and $p' = p$, is obtained as

$$\frac{dp'}{dt'} = e\left[\mathscr{E}_o + \mathscr{E}_1 \cos\left(\omega t'\right)\right], \tag{5}$$

which has a solution given as

$$p' = e\mathscr{E}_o t' + \frac{e\mathscr{E}_1}{\omega}\left[\sin\left(\omega t'\right) - \sin\left[\omega\left(t - t'\right)\right]\right]. \tag{6}$$

One issue that needs to be addressed prior to obtaining a solution for the BTE is how to manage the collision term located on the RHS of (4). The standard approach involves employing the relaxation time ansatz. In this context, the assumption is that when all external forces are deactivated, the distribution function will gradually return to a suitable equilibrium distribution $F_o(p)$, within a time interval τ. This ansatz has been examined and found to be quite effective when the primary scattering processes are elastic, as is the case with impurity scattering, and when τ is independent of the electric and magnetic fields. This ansatz has extensive application in the computation of the absorption coefficient for acoustic waves interacting with carriers, yielding favourable outcomes when compared to experimental data. Thus, employing the relaxation time ansatz, (4) becomes

$$\frac{\partial F(r,p,t)}{\partial t} + v \cdot \frac{\partial F(r,p,t)}{\partial r} + e\left[\mathscr{E}_o + \mathscr{E}_1 \cos\left(\omega t\right)\right]\frac{\partial F(r,p,t)}{\partial p} = -\frac{F(r,p,t) - F_S(p,t)}{\tau}. \tag{7}$$

The distribution function to which the carriers relax in the presence of the acoustic wave $F_S(p)$ is not necessarily the same as the equilibrium distribution function in the absence of the wave $F_o(p)$. If the dominant scattering mechanism for the carriers is from impurities, as is usually the case at low temperatures, or from acoustic phonons, as is the case at high temperatures, then the carriers relax to an equilibrium distribution in the rest frame of the moving lattice.

The BTE is solved by using Chambers' approach. In this method, a carrier contributes to the distribution function $F(r, p, t)$ only if it is at a point (r, p) in phase space at time t. The number of carriers scattered in a time dt' and at a point (r', p') on a trajectory that goes through this point in phase space is $F_S(r', p', t')dt'$. To obtain the probability that the carrier will reach this point in phase space, we multiply the number scattered onto a trajectory going through this point by the probability that the carrier will not scatter again and integrates over all time up to t. By ignoring the spatial distribution, the nonequilibrium distribution function is obtained as

$$F(p,t) = \int_0^\infty \frac{dt'}{\tau}\exp\left[-\left(\frac{t-t'}{\tau}\right)\right]F_S\left(p,t'\right), \tag{8}$$

where $F_S\left(p, t'\right)$ is the distribution in the presence of acoustic phonons and electric field. Performing the transformation $p \longrightarrow p - p'$, the solution to the BTE, is found by assuming τ to be constant as

$$F(p,t) = \int_0^\infty \frac{dt'}{\tau}\exp\left(\frac{-t'}{\tau}\right)F_o\left[p + q - \left(e\mathscr{E}_o t' + \frac{e\mathscr{E}_1}{\omega}\left[\sin\left(\omega t'\right) - \sin\left[\omega\left(t - t'\right)\right]\right]\right)\right]. \tag{9}$$

When the acoustic phonons and electric field are switched off, the Fermi–Dirac function reduces Boltzmann's function for a nondegenerate carrier gas where the Fermi level is several times below the energy of the band edge ϑ_c (i.e., $\mathscr{T} \ll \vartheta_c$) as follows:

$$F_o(p) = A^\dagger \exp\left[\frac{\Delta_s}{\mathscr{T}}\cos\left(\frac{p_s d_s}{\hbar}\right) + \frac{\Delta_z}{\mathscr{T}}\cos\left(\frac{p_z d_z}{\hbar}\right) - \left(\frac{\varrho - \vartheta_o}{\mathscr{T}}\right)\right], \tag{10}$$

where $\mathscr{T} = kT$ is the temperature in energy unit, k is Boltzmann's constant, and $\mathscr{E}_o$, $\mathscr{E}_1$, and ϱ represent the constant dc field, ac field, and carriers' electrochemical potential, respectively. $A^\dagger$ is the normalisation constant determined using the normalisation condition to be [46, 47, 50]:

$$A^\dagger = \frac{n_o d_s d_z}{2I_o\left(\Delta_s^*\right)I_o\left(\Delta_z^*\right)}\exp\left(\frac{\varrho - \vartheta_o}{\mathscr{T}}\right), \tag{11}$$

where n_o is the carrier concentration and $I_n(x)$ is a modified Bessel function of order n. Substituting (9)–(11) into (1) yields

$$\begin{aligned} J = {} & \frac{e\Phi\Lambda^2 q^2 \tau A^{\dagger}}{(2\pi\hbar)^2 \rho v_s \omega_q} \sum_p \exp\left(\frac{\Delta_z}{\mathscr{T}}\cos\left(\frac{p_z d_z}{\hbar}\right)\right) \\ & \times \int_0^{\infty} e^{-t'/\tau}\frac{dt'}{\tau}\left[\exp\left(\frac{\Delta_s}{\mathscr{T}}\cos\left(p_s - e\mathscr{E}_o t' - \frac{e\mathscr{E}_1}{\omega}\left[\sin(\omega t') - \sin[\omega(t-t')]\right]\right)d_s\right)\right. \\ & \left. - \exp\left(\frac{\Delta_s}{\mathscr{T}}\cos\left(p_s + q - e\mathscr{E}_o t' - \frac{e\mathscr{E}_1}{\omega}\left[\sin(\omega t') - \sin[\omega(t-t')]\right]\right)d_s\right)\right] \\ & \cdot \left[v_s(p_s+q) - v_s(p_s)\right]\delta\left(\frac{\omega_q}{2\Delta_s \sin(qd_s/2)} - \sin\left(p_s + \frac{q}{2}\right)\right). \end{aligned} \tag{12}$$

Within the first Brillouin zone, we use the following transformation to change the summation over p into an integral over p as

$$\sum_p \longrightarrow \frac{2}{(2\pi\hbar)^2}\int_{-\pi/d_s}^{\pi/d_s} dp_s \int_{-\pi/d_z}^{\pi/d_z} dp_z, \tag{13}$$

and the acoustoelectric current density takes the form

$$\begin{aligned} J = {} & \frac{e\Phi\Lambda^2 q^2 \tau A^{\dagger}}{(2\pi\hbar)^2 \rho v_s \omega_q} \int_{-\pi/d_z}^{\pi/d_z} \exp\left(\frac{\Delta_z}{\mathscr{T}}\cos\left(\frac{p_z d_z}{\hbar}\right)\right) dp_z \\ & \times \int_0^{\infty} e^{-t'/\tau}\frac{dt'}{\tau}\left[\exp\left(\frac{\Delta_s}{\mathscr{T}}\cos\left(p_s - e\mathscr{E}_o t' - \frac{e\mathscr{E}_1}{\omega}\left[\sin(\omega t') - \sin[\omega(t-t')]\right]\right)d_s\right)\right. \\ & \left. - \exp\left(\frac{\Delta_s}{\mathscr{T}}\cos\left(p_s + q - e\mathscr{E}_o t' - \frac{e\mathscr{E}_1}{\omega}\left[\sin(\omega t') - \sin[\omega(t-t')]\right]\right)d_s\right)\right] \\ & \cdot \left[v_z(p_z+q) - v_z(p_z)\right]\delta\left(\frac{\omega_q}{2\Delta_s \sin(qd_s/2)} - \sin\left(p_s + \frac{q}{2}\right)\right), \end{aligned} \tag{14}$$

and the carrier current densities along the base helix ($\mathscr{S}$) and tubular ($\mathscr{Z}$) directions are obtained as follows [46, 47, 50]:

$$\begin{aligned} \mathscr{S} = {} & -\frac{e\Phi\Lambda^2 q^2 \tau A^{\dagger}}{(2\pi\hbar)^2 \rho v_s \omega_q} \int_{-\pi/d_z}^{\pi/d_z} \exp\left(\frac{\Delta_z}{\mathscr{T}}\cos\left(\frac{p_z d_z}{\hbar}\right)\right) dp_z \\ & \times \int_0^{\infty} e^{-t'/\tau}\frac{dt'}{\tau}\left[\exp\left(\frac{\Delta_s}{\mathscr{T}}\cos\left(p_s - e\mathscr{E}_o t' - \frac{e\mathscr{E}_1}{\omega}\left[\sin(\omega t') - \sin[\omega(t-t')]\right]\right)d_s\right)\right. \\ & \left. - \exp\left(\frac{\Delta_s}{\mathscr{T}}\cos\left(p_s + q - e\mathscr{E}_o t' - \frac{e\mathscr{E}_1}{\omega}\left[\sin(\omega t') - \sin[\omega(t-t')]\right]\right)d_s\right)\right] \\ & \cdot \left[v_z(p_z+q) - v_z(p_z)\right]\delta\left(\frac{\omega_q}{2\Delta_s \sin(qd_s/2)} - \sin\left(p_s + \frac{q}{2}\right)\right), \end{aligned} \tag{15}$$

and

$$\begin{aligned}\mathscr{Z} = &-\frac{e\Phi\Lambda^2 q^2 \tau A^{\dagger}}{(2\pi\hbar)^2 \rho v_s \omega_q} \int_{-\pi/d_s}^{\pi/d_s} \exp\left(\frac{\Delta_s}{\mathscr{T}} \cos\left(\frac{p_s d_s}{\hbar}\right)\right) dp_s \\ &\times \int_0^{\infty} e^{-t'/\tau} \frac{dt'}{\tau} \left[\exp\left(\frac{\Delta_z}{\mathscr{T}} \cos\left(p_z - e\mathscr{E}_o t' - \frac{e\mathscr{E}_1}{\omega}\left[\sin(\omega t') - \sin[\omega(t-t')]\right]\right) d_z\right)\right. \\ &\left. - \exp\left(\frac{\Delta_s}{\mathscr{T}} \cos\left(p_z + q - e\mathscr{E}_o t' - \frac{e\mathscr{E}_1}{\omega}\left[\sin(\omega t') - \sin[\omega(t-t')]\right]\right) d_z\right)\right] \\ &\cdot \left[v_z(p_z+q) - v_z(p_z)\right] \delta\left(\frac{\omega_q}{2\Delta_z \sin(q d_z/2)} - \sin\left(p_z + \frac{q}{2}\right)\right).\end{aligned} \tag{16}$$

The carrier momenta for the base helix and tubular directions in the first and second quadrants of the first Brillouin zone in the presence of the acoustic phonons are determined as in [52]:

$$p_s^1 = \frac{1}{d_s}\sin^{-1}\left(\frac{\omega_q}{2\Delta_s \sin(q d_s/2)}\right) - \frac{q}{2} \quad p_s^2 = \frac{\pi}{d_s} - \frac{\pi}{d_s}\sin^{-1}\left(\frac{\omega_q}{2\Delta_s \sin(q d_s/2)}\right) - \frac{q}{2}, \tag{17}$$

$$p_z^1 = \frac{1}{d_z}\sin^{-1}\left(\frac{\omega_q}{2\Delta_z \sin(q d_z/2)}\right) - \frac{q}{2} \quad p_z^2 = \frac{\pi}{d_z} - \frac{\pi}{d_z}\sin^{-1}\left(\frac{\omega_q}{2\Delta_z \sin(q d_z/2)}\right) - \frac{q}{2}. \tag{18}$$

Equations (17) and (18) are substituted into (15) and (16), and conventional integrals are used to obtain the acoustoelectric carrier current densities along the base helix ($\mathscr{S}$) and tubular ($\mathscr{Z}$):

$$\begin{aligned}\mathscr{S} = &-\frac{e\Phi\Lambda^2 q^2 \tau n_o d_s^2 d_z \theta\left(1-\alpha_s^2\right)}{(\pi\hbar)^2 \rho v_s \omega_q \cdot \Delta_s \sin(q d_s/2)\sqrt{1-\alpha_s^2} I_o(\Delta_s/\mathscr{T})} \\ &\times \int_0^{\infty} e^{-t'/\tau} \frac{dt'}{\tau} \left[\sinh\left(\frac{\Delta_s}{\mathscr{T}} \sin A \cos B \sin\left(\frac{q d_s}{2}\right)\right) \sinh\left(\frac{\Delta_s}{\mathscr{T}} \cos A \cos B \cos\left(\frac{q d_s}{2}\right)\right)\right. \\ &\left. - \frac{\Delta_s}{\mathscr{T}} \cos A \sin B \sin\left(\frac{q d_s}{2}\right) \cosh\left(\frac{\Delta_s}{\mathscr{T}} \cos A \cos B \cos\left(\frac{q d_s}{2}\right)\right) \cosh\left(\frac{\Delta_s}{\mathscr{T}} \sin A \cos B \sin\left(\frac{q d_s}{2}\right)\right)\right], \\ \mathscr{Z} = &-\frac{e\Phi\Lambda^2 q^2 \tau n_o d_s d_z^2 \theta\left(1-\alpha_z^2\right)}{(\pi\hbar)^2 \rho v_s \omega_q \cdot \Delta_z \sin(q d_z/2)\sqrt{1-\alpha_z^2} I_o(\Delta_z/\mathscr{T})} \\ &\times \int_0^{\infty} e^{-t'/\tau} \frac{dt'}{\tau} \left[\sinh\left(\frac{\Delta_z}{\mathscr{T}} \sin A \cos B \sin\left(\frac{q d_z}{2}\right)\right) \sinh\left(\frac{\Delta_z}{\mathscr{T}} \cos A \cos B \cos\left(\frac{q d_z}{2}\right)\right)\right. \\ &\left. - \frac{\Delta_z}{\mathscr{T}} \cos A \sin B \sin\left(\frac{q d_z}{2}\right) \cosh\left(\frac{\Delta_z}{\mathscr{T}} \cos A \cos B \cos\left(\frac{q d_z}{2}\right)\right) \cosh\left(\frac{\Delta_z}{\mathscr{T}} \sin A \cos B \sin\left(\frac{q d_z}{2}\right)\right)\right],\end{aligned} \tag{19}$$

where θ is the Heaviside step function. For $\mathscr{T} \gg \Delta_s$ and $\mathscr{T} \gg \omega_q$,

$$\mathcal{S} = -\frac{e\Phi\Lambda^2 q^2 \tau n_o d_s^2 d_z \theta\left(1-\alpha_s^2\right)}{(\pi\hbar)^2 \rho v_s \omega_q \cdot \Delta_s \sin\left(qd_s/2\right)\sqrt{1-\alpha_s^2} I_o\left(\Delta_s/\mathcal{T}\right)} \times \int_0^\infty e^{-t'/\tau}\frac{dt'}{\tau}\left[\left(\frac{\Delta_s}{\mathcal{T}}\right)^2 \sin A\cos A \sin\left(\frac{qd_s}{2}\right)\cos\left(\frac{qd_s}{2}\right)\cos^2 B - \frac{\Delta_s}{\mathcal{T}}\cos A \sin B \sin\left(\frac{qd_s}{2}\right)\right], \tag{20}$$

and

$$\mathcal{Z} = -\frac{e\Phi\Lambda^2 q^2 \tau n_o d_s d_z^2 \theta\left(1-\alpha_z^2\right)}{(\pi\hbar)^2 \rho v_s \omega_q \cdot \Delta_s \sin\left(qd_z/2\right)\sqrt{1-\alpha_z^2} I_o\left(\Delta_z/\mathcal{T}\right)} \times \int_0^\infty e^{-t'/\tau}\frac{dt'}{\tau}\left[\left(\frac{\Delta_z}{\mathcal{T}}\right)^2 \sin A\cos A \sin\left(\frac{qd_z}{2}\right)\cos\left(\frac{qd_z}{2}\right)\cos^2 B - \frac{\Delta_z}{\mathcal{T}}\cos A \sin B \sin\left(\frac{qd_z}{2}\right)\right], \tag{21}$$

where

$$B = e\mathcal{E}_o d_s t' + \frac{e\mathcal{E}_1 d_s}{\omega}\left[\sin\left(\omega t'\right) - \sin\left[\omega\left(t-t'\right)\right]\right]. \tag{22}$$

Equations (20) and (21) further reduce to

$$\mathcal{S} = J_{os}\int_0^\infty e^{-t'/\tau}\frac{dt'}{\tau}\left[\cos^2 B - \frac{4\mathcal{T}\cos A \sin\left(qd_z/2\right)}{\Delta_s}\sin B\right],$$
$$\mathcal{Z} = J_{oz}\int_0^\infty e^{-t'/\tau}\frac{dt'}{\tau}\left[\cos^2 B - \frac{4\mathcal{T}\cos A \sin\left(qd_z/2\right)}{\Delta_z}\sin B\right]. \tag{23}$$

Making use of the identity, $\cos^2(x) = 1/2\,(1+\cos(2x))$ yields

$$\mathcal{S} = J_{os}\int_0^\infty e^{-t'/\tau}\frac{dt'}{\tau}\left[\frac{1}{2}\left(1+e^{i2e\mathcal{E}_o d_s t'}\mathcal{R}e\left[e^{iz'\left(\sin\omega t - \sin\omega\left(t-t'\right)\right)}\right]\right) - \frac{4\mathcal{T}\cos A\sin\left(qd_s/2\right)}{\Delta_s}\mathcal{I}m\left[e^{iz\left(\sin\omega t - \sin\omega\left(t-t'\right)\right)}\right]\right],$$
$$\mathcal{Z} = J_{oz}\int_0^\infty e^{-t'/\tau}\frac{dt'}{\tau}\left[\frac{1}{2}\left(1+e^{i2e\mathcal{E}_o d_s t'}\mathcal{R}e\left[e^{iz'\left(\sin\omega t - \sin\omega\left(t-t'\right)\right)}\right]\right) - \frac{4\mathcal{T}\cos A\sin\left(qd_z/2\right)}{\Delta_z}\mathcal{I}m\left[e^{iz\left(\sin\omega t - \sin\omega\left(t-t'\right)\right)}\right]\right]. \tag{24}$$

Solving explicitly gives

$$\mathcal{S} = \frac{J_{os}}{2}\left(1+\sum_{k=-\infty}^{\infty}\frac{J_k^2\left(z'\right)}{1+\left(2\Omega\tau+k\omega\tau\right)^2} - \frac{8\cos A\sin\left(qd_s/2\right)}{\Delta_s}\sum_{k=-\infty}^{\infty}\frac{J_k^2\left(z\right)\left(\Omega\tau+k\omega\tau\right)}{1+\left(\Omega\tau+k\omega\tau\right)^2}\right),$$
$$\mathcal{Z} = \frac{J_{oz}}{2}\left(1+\sum_{k=-\infty}^{\infty}\frac{J_k^2\left(z'\right)}{1+\left(2\Omega\tau+k\omega\tau\right)^2} - \frac{8\cos A\sin\left(qd_z/2\right)}{\Delta_s}\sum_{k=-\infty}^{\infty}\frac{J_k^2\left(z\right)\left(\Omega\tau+k\omega\tau\right)}{1+\left(\Omega\tau+k\omega\tau\right)^2}\right). \tag{25}$$

where

$$J_{os} = -\frac{e\Phi\Lambda^2 q^2 \tau n_o d_s^2 d_z \theta\left(1-\alpha_s^2\right)\Delta_s^2 \sin(2A)\sin\left(qd_s\right)}{4\mathscr{T}\pi\hbar^2\rho v_s \omega_q \sin\left(qd_s/2\right)\sqrt{1-\alpha_s^2} I_o\left(\Delta_s/\mathscr{T}\right)},$$

$$J_{oz} = -\frac{e\Phi\Lambda^2 q^2 \tau n_o d_s d_z^2 \theta\left(1-\alpha_z^2\right)\Delta_z^2 \sin(2A)\sin\left(qd_z\right)}{4\mathscr{T}\pi\hbar^2\rho v_s \omega_q \sin\left(qd_z/2\right)\sqrt{1-\alpha_z^2} I_o\left(\Delta_z/\mathscr{T}\right)}. \tag{26}$$

The development of the chiral current, a distinctive feature distinguishing FSWCNTs from zigzag and armchair SWCNTs, is a key characteristic [53, 54]. An axial electric field compels the current to follow a helical path. We use the labels $\mathscr{Z}$ and $\mathscr{S}$ to denote the axial and azimuthal components of the surface current density, respectively. Miyamoto et al. conducted a first-principle numerical simulation of the chiral current, while elsewhere, researchers employed phenomenological modeling [53–56]. Both approaches reached the same conclusion: chiral conductivity is relatively low compared to axial conductivity. To maintain generality, we decompose the high-frequency acoustoelectric current density into axial and circumferential components as follows: $\vec{J}_z = \vec{\mathscr{Z}}_q + \vec{\mathscr{S}}_q \sin\theta_h$ and $\vec{J}_s = \vec{\mathscr{S}}_q \cos\theta_h$, respectively. The expression for the axial carrier thermal current density is given as

$$\begin{aligned} J_z = {} & \frac{J_{oz}}{2}\left(1 + \sum_{k=-\infty}^{\infty} \frac{J_k^2(z')}{1+(2\Omega\tau + k\omega\tau)^2} - \frac{8\cos A \sin\left(qd_z/2\right)}{\Delta_s} \sum_{k=-\infty}^{\infty} \frac{J_k^2(z)(\Omega\tau + k\omega\tau)}{1+(\Omega\tau + k\omega\tau)^2}\right) \\ & + \frac{J_{os}}{2}\left(1 + \sum_{k=-\infty}^{\infty} \frac{J_k^2(z')}{1+(2\Omega\tau + k\omega\tau)^2} - \frac{8\cos A \sin\left(qd_s/2\right)}{\Delta_s} \sum_{k=-\infty}^{\infty} \frac{J_k^2(z)(\Omega\tau + k\omega\tau)}{1+(\Omega\tau + k\omega\tau)^2}\right)\sin^2\vartheta, \end{aligned} \tag{27}$$

and

$$J_s = \frac{J_{os}}{2}\left(1 + \sum_{k=-\infty}^{\infty} \frac{J_k^2(z')}{1+(2\Omega\tau + k\omega\tau)^2} - \frac{8\cos A \sin\left(qd_s/2\right)}{\Delta_s} \sum_{k=-\infty}^{\infty} \frac{J_k^2(z)(\Omega\tau + k\omega\tau)}{1+(\Omega\tau + k\omega\tau)^2}\right)\cos\vartheta\sin\vartheta, \tag{28}$$

where $z' = 2z = 2e\mathscr{E}_1 d_s/\omega$ and $\Omega_o = \Omega = e\mathscr{E}_o d_{s,z}$.

(i) For $z' \ll 1$ and $z \ll 1$, then $J_{\pm} \approx (z/2)^2$ and $J_o \approx 1 - z^2/2$; thus,

$$\begin{aligned} J_z &= \frac{J_{oz}}{2}\left(1 + \mathscr{A} - \frac{8\cos A \sin\left(qd_z/2\right)}{\Delta_z}\mathscr{B}\right) + \frac{J_{os}}{2}\left(1 + \mathscr{A} - \frac{8\cos A \sin\left(qd_s/2\right)}{\Delta_s}\mathscr{B}\right)\sin^2\vartheta, \\ J_s &= \frac{J_{os}}{2}\left(1 + \mathscr{A} - \frac{8\cos A \sin\left(qd_s/2\right)}{\Delta_s}\mathscr{B}\right)\cos\vartheta\sin\vartheta, \end{aligned} \tag{29}$$

where

$$\mathscr{A} = \frac{\left(1 - z'^2/2\right)\left[1 + (2\Omega + \omega)^2\tau^2\right]\left[1 + (2\Omega - \omega)^2\tau^2\right] + \left(z'/2\right)^2\left[1 + (2\Omega)^2\tau^2\right]\left[1 + (2\Omega - \omega)^2\tau^2\right]}{\left[1 + (2\Omega)^2\tau^2\right]\left[1 + (2\Omega - \omega)^2\tau^2\right]\left[1 + (2\Omega + \omega)^2\tau^2\right]}$$
$$+ \frac{\left(z'/2\right)^2\left[1 + (2\Omega)^2\tau^2\right]\left[1 + (2\Omega + \omega)^2\tau^2\right]}{\left[1 + (2\Omega)^2\tau^2\right]\left[1 + (2\Omega - \omega)^2\tau^2\right]\left[1 + (2\Omega + \omega)^2\tau^2\right]},$$
$$\mathscr{B} = \frac{\left(1 - z'^2/2\right)\left[1 + (\Omega + \omega)^2\tau^2\right]\left[1 + (\Omega - \omega)^2\tau^2\right] + \left(z'/2\right)^2\left[1 + (2\Omega)^2\tau^2\right]\left[1 + (\Omega - \omega)^2\tau^2\right]}{\left[1 + (\Omega)^2\tau^2\right]\left[1 + (\Omega - \omega)^2\tau^2\right]\left[1 + (\Omega + \omega)^2\tau^2\right]} \tag{30}$$
$$+ \frac{\left(z'/2\right)^2\left[1 + (\Omega)^2\tau^2\right]\left[1 + (\Omega + \omega)^2\tau^2\right]}{\left[1 + (\Omega)^2\tau^2\right]\left[1 + (\Omega - \omega)^2\tau^2\right]\left[1 + (\Omega + \omega)^2\tau^2\right]},$$

(ii) For $z' = z = 0$ [57],

$$J_z = \frac{J_{oz}}{2}\left(1 + \frac{1}{1 + (2\Omega\tau)^2} - \frac{8\cos A \sin\left(qd_z/2\right)}{\Delta_s}\frac{(\Omega\tau)}{1 + (\Omega\tau)^2}\right)$$
$$+ \frac{J_{os}}{2}\left(1 + \frac{1}{1 + (2\Omega\tau)^2} - \frac{8\cos A \sin\left(qd_s/2\right)}{\Delta_s}\frac{(\Omega\tau)}{1 + (\Omega\tau)^2}\right)\sin^2\vartheta, \tag{31}$$
$$J_s = \frac{J_{os}}{2}\left(1 + \frac{1}{1 + (2\Omega\tau)^2} - \frac{8\cos A \sin\left(qd_s/2\right)}{\Delta_s}\frac{(\Omega\tau)}{1 + (\Omega\tau)^2}\right)\cos\vartheta\sin\vartheta,$$

when $\Omega\tau \ll 1$, i.e., in a linear approx. to $\mathscr{E}_0$

$$\mathscr{E} > \mathscr{E}_0^{\mathrm{FSWCNT}} = \frac{\Delta_{s,z}}{4ed_{s,z}\tau\cos A \sin\left(qd_{s,z}/2\right)}. \tag{32}$$

Furthermore, when $\Omega\tau \gg 1$,

$$\mathscr{E}_0^{\mathrm{FSWCNT}} = \frac{\Delta_{s,z}}{8ed_{s,z}\tau\cos A \sin\left(qd_{s,z}/2\right)}. \tag{33}$$

(iii) For $\mathscr{E}_o = 0$,

$$J_z = \frac{J_{oz}}{2}\left(1 + \sum_{k=-\infty}^{\infty}\frac{J_k^2(z')}{1 + (k\omega\tau)^2} - \frac{8\cos A \sin\left(qd_z/2\right)}{\Delta_s}\sum_{k=-\infty}^{\infty}\frac{J_k^2(z)\,(k\omega\tau)}{1 + (\Omega\tau + k\omega\tau)^2}\right)$$
$$+ \frac{J_{os}}{2}\left(1 + \sum_{k=-\infty}^{\infty}\frac{J_k^2(z')}{1 + (k\omega\tau)^2} - \frac{8\cos A \sin\left(qd_s/2\right)}{\Delta_s}\sum_{k=-\infty}^{\infty}\frac{J_k^2(z)\,(k\omega\tau)}{1 + (\Omega\tau + k\omega\tau)^2}\right)\sin^2\vartheta, \tag{34}$$
$$J_s = \frac{J_{os}}{2}\left(1 + \sum_{k=-\infty}^{\infty}\frac{J_k^2(z')}{1 + (k\omega\tau)^2} - \frac{8\cos A \sin\left(qd_s/2\right)}{\Delta_s}\sum_{k=-\infty}^{\infty}\frac{J_k^2(z)\,(k\omega\tau)}{1 + (\Omega\tau + k\omega\tau)^2}\right)\cos\vartheta\sin\vartheta.$$

We can set only $k = 0$:

$$J_z = \frac{J_{oz}}{2}\left(1 + J_0^2(z')\right) + \frac{J_{os}}{2}\left(1 + J_0^2(z')\right)\sin^2\vartheta,$$
$$J_s = \frac{J_{os}}{2}\left(1 + J_0^2(z')\right)\cos\vartheta\sin\vartheta. \quad (35)$$

The high-frequency acoustoelectric current density relies on the amplitude of the ac electric field in an oscillatory fashion. In the limit $z' \gg 1$ and $z \gg 1$,

$$J_z = \frac{J_{oz}}{2}\left(1 + \cos^2\left[\frac{2e\mathscr{E}_1 d_z}{\omega} - \frac{\pi}{4}\right]\right) + \frac{J_{os}}{2}\left(1 + \cos^2\left[\frac{2e\mathscr{E}_1 d_s}{\omega} - \frac{\pi}{4}\right]\right)\sin^2\vartheta,$$
$$J_s = \frac{J_{os}}{2}\left(1 + \cos^2\left[\frac{2e\mathscr{E}_1 d_s}{\omega} - \frac{\pi}{4}\right]\right)\cos\vartheta\sin\vartheta. \quad (36)$$

This is similar to that of acoustoelectric current in a quantised electric field. This is not accidental because in a quantised electric field, carriers undergo Stark oscillations, while in our case, an ac field undergoes harmonic oscillations [57].

3. Results and Discussion

The acoustic phonons to be examined in this investigation have a wavelength denoted as $\lambda = 2\pi/q$, which is shorter than the mean-free path (ℓ) of FSWCNT carriers within the hypersound region where $q\ell \gg 1$. In this context, the acoustic wave is treated as the packet of coherent phonons, essentially monochromatic phonons, characterised by a δ-function distribution given as

$$N(\vec{k}) = \frac{(2\pi)^3}{\hbar\omega_q v_s}\vec{\Phi}\delta(\vec{k} - \vec{q}). \quad (37)$$

Note that $\vec{k}$ represents the electron wavevector, $\hbar$ denotes the reduced Planck's constant, $\vec{\Phi}$ signifies the sound flux density, and ω_q and v_s correspond to the frequency and group velocity of sound waves characterised by the wavevector $\vec{q}$.

Equations (27) and (28) present the general equations describing the acoustoelectric current density in FSWCNT with a primary focus directed toward the axial component outlined in (27). A numerical analysis of (27) was conducted using the following set of parameters: $\omega_q = 10^{11}\,\mathrm{s}^{-1}$, $v_s = 2.5 \times 10^3$ m/s, $\Phi = 10^5\,\mathrm{Wb/m}^2$, $q = 10^6\,cm^{-1}$, $\lambda = 10^{-5}\,cm^{-1}$, and $\ell = 10^{-4}\,cm$. The acoustic current generated in both cases is observed to be strongly dependent on the acoustic wavenumber (q), frequency (ω_q), temperature (T), and external field ($\mathscr{E}$). A transparency window is observed when $\omega_q \gg 2\Delta_s \sin(qd_s/2)$ and $\omega_q \gg 2\Delta_s \sin(qd_z/2)$, which is a consequence of the conservation laws of energy and momentum. It follows then that only carriers with momenta $\hbar q/2$ interact with the acoustic phonons. If the phonon flux passing through the FSWCNT has a frequency which is extremely high, there will be no absorption of phonons and the acoustoelectric current density (J_{zz}^{ae}/J_o^{ae}) will be zero.

Figure 1 shows the normalised acoustoelectric direct current density (J_{zz}^{ae}/J_o^{ae}) dependency on the dimensionless electric field ($\Omega\tau$) in the region of $\omega\tau \ll 1$ and $z < 1$. The current density is observed to be complex and highly anisotropic.

To understand how the various parameters affects J_{zz}^{ae}/J_o^{ae} dependency on $\Omega\tau$, we look at the physics of the carrier behaviour exhibited in Figure 1. When $\mathscr{E}_o$ is negative, the carriers are trapped by the acoustic waves, dragged, and move in the direction of the acoustic waves, while the acoustic waves interact strongly with the holes to generate the hole current. This interaction results in the generation of a current carried by either electrons or holes, depending on the polarity of the electric field. Conversely, when the external electric field $\mathscr{E}_o$ is positive, the opposite behaviour occurs. The carriers (either electrons or holes) are trapped and dragged by the acoustic waves in the direction of the waves. This time, the acoustic waves interact strongly with the opposite type of carrier (electrons or holes) compared to the previous case, which results in the generation of a current carried by the opposite type of carrier. The basic idea is undoubtedly the proof that for a sufficiently large dc force amplitude, the differential dc conductivity becomes positive over a range of negative dc bias values where a range of positive dc bias conductivity is negative. Therefore, there is a good likelihood that domain suppression and acoustic Bloch gain will be applied in purely dynamic dc stabilisation.

It is inferred from this behaviour that the dynamic complex current density is initially positive and becomes more positive with increasing dc electric field ($\Omega\tau$), until it reaches resonance maximum enhancement at a frequency (i.e., Bloch frequency) somewhat below the critical dc electric field ($\Omega\tau$), which turns negative and becomes more negative, until it again reaches negative resonant minimum enhancement and turns positive again. This observed behaviour is attributed to Bragg reflection of the carriers at the band edges due to the Umklapp process the carriers are subjected to and results in Bloch oscillations of the carriers.

In order to suppress the electric field domains cause by the onset of NDV (and NDC), the negative minimum resonant enhancement should make it possible to suppress any domain instabilities induced by any NDV (and NDC) at low frequencies with positive conductance that is sufficiently high to make the acoustoelectric dc conductivity positive, without destruction of NDV (and NDC) just below the critical dc field $\mathscr{E}_o^c$.

Space charge instabilities can also be suppressed if the ac part of the drive field is kept so strong ($\omega\tau \gg 1$) that the overall field dips, during each cycle, to very low values at which the static velocity-field-characteristic has a steep positive slope. Under steady-state operation at such negative dc fields, the FSWCNT will be an "ordinary" conductor with positive conductivity, and any space charges will decay when dc is negative rather than build up. Given a suitable combination of the dc and ac operating conditions, domains are unable to build up much. Similar dynamic stabilisation can also be achieved when the high-frequency component of the drive field builds up to values that are no longer small compared to the dc component.

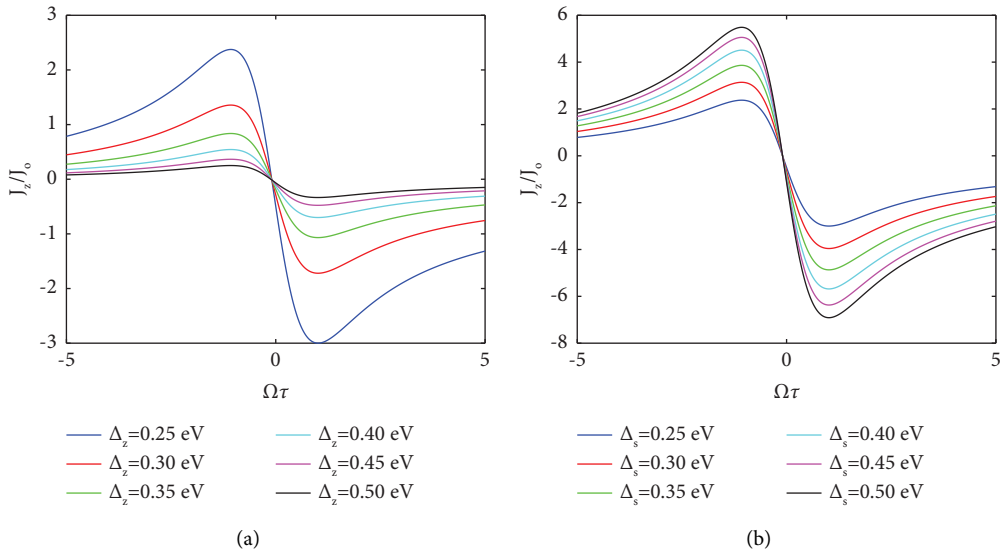

FIGURE 1: Dependence of acoustoelectric current (J_{zz}^{ae}/J_o^{ae}) on $\Omega\tau$ for different values: (a) Δ_z with $\Delta_s = 0.25$ eV, $\omega\tau = 0.5$, $z = 0.5$; (b) Δ_s with $\Delta_z = 0.25$ eV, $\omega\tau = 0.5$, $z = 0.5$.

We however observe from Figure 1(a) that when Δ_z is varied and Δ_s is fixed $(\Delta_s = 0.25eV)$, the acoustoelectric current increases in both directions than in Figure 1(b) when Δ_s is varied and Δ_z is fixed $(\Delta_s = 0.25eV)$ [59–61]. This again is attributed to scattering of carriers which is low along Δ_s (see Figure 1(a)) than Δ_z (see Figure 1(b)). The FSWCNT's current-voltage characteristic (see Figure 1) is essentially antisymmetric. The current is proportionate to the voltage in both bias directions until it reaches a resonance maximum (or minimum). A further increase in voltage results in a drop in ADC, which indicates the onset of NDV (and NDC). NDV (and NDC) begins at a critical voltage $U_c = 1.0\,V/-1.07\,V$ (see Figures 1(a) and 1(b)) where $\mathscr{E}_o = U/L$. ADC displays both gradual and sudden variations above U, indicating a space charge instability and a nonstatic electric field. The current reduces significantly in the NDV (and NDC) ranges, as expected for a homogenous electric field distribution [1]. We suggest that this can also be due to the suppression of space charge instability by the ac component of the external field. We however observe THz emissions from the FSWCNT throughout the NDV (and NDC) regions.

We display in Figure 2 the normalised acoustoelectric current density (J_{zz}^{ae}/J_o^{ae}) dependency on the dimensionless electric field $(\Omega\tau)$ in the region of strong ac field (i.e., $\omega\tau \gg 1$) but not strong enough to quantise the FSWCNT band structure. In the presence $\omega\tau \gg 1$ and $z > 1$, the peak values of J_{zz}^{ae}/J_o^{ae} begin to fall (see Figure 2(a)) but oscillate harmonically with more enhancements as the dc electric field $(\Omega\tau)$ becomes more positive when Δ_z is varied and Δ_s is fixed $(\Delta_s = 0.25eV)$. However, when Δ_s is varied and Δ_z is fixed $(\Delta_s = 0.25eV)$, J_{zz}^{ae}/J_o^{ae} dependency on $\Omega\tau$ increases but with similar behaviour as observed in Figure 2(b). The ac field in this case acts as a modulator and modulates the dc field by updating the momenta and kinetic energies of carriers that has less energy to interact with the acoustic phonons. To enhance J_{zz}^{ae}/J_o^{ae}, the majority of carriers with requisite momenta and energies interacted strongly with the acoustic phonons and performed intraminiband transition and generated a large intraminiband current (see Figures 2(a) and 2(b)). ADC shows both smooth and abrupt changes giving evidence for a strong space charge instability and a nonstatic electric field in the nondegenerate FSWCNT (i.e., $\omega\tau \gg 1$).

Herein, we examine in Figure 3 the normalised acoustoelectric current density (J_{zz}^{ae}/J_o^{ae}) dependency on the dimensionless electric field $(\Omega\tau)$ when z is varied and $\omega\tau$ is fixed. In Figures 3(a) and 3(b), we display J_{zz}^{ae}/J_o^{ae} dependency on $\Omega\tau$ when $\omega\tau = 0$ (see Figure 3(a)) and $\omega\tau = 0.5$ (see Figure 3(b)). There is minimal or no change observed in J_{zz}^{ae}/J_o^{ae} when $\omega\tau = 0$ and z is varied between $z = 0$ and $z = 0.5$. However, J_{zz}^{ae}/J_o^{ae} starts to decrease drastically from $z = 1.5 - 3.0$ (see Figure 3(a)). Similar behaviour is observed in Figure 3(b), but the change observed when z is varied for fixed $\omega\tau = 0.5$ is a bit clearer in Figure 3(b) than in 3(a). Furthermore, when $z \gg 0$, $\omega\tau = 1$, and $\omega\tau = 1.5$ for Figures 3(c) and 3(d), respectively, we observe that J_{zz}^{ae}/J_o^{ae} dependency on $\Omega\tau$ begins to fall gradually but oscillates much more strongly harmonically in Figure 3(b) than observed in 3(a).

Figure 4 displays the normalised acoustoelectric current density (J_{zz}^{ae}/J_o^{ae}) dependency on the dimensionless electric field $(\Omega\tau)$ for varied values of n_o in different dynamic regimes. The J_{zz}^{ae}/J_o^{ae} dependency on $\Omega\tau$ increases gradually when the impurity concentration n_o increases in the region of $\Delta_s = \Delta_z = 0.25eV$, $\omega\tau = 0.5$, and $z = 0.5$. This high J_{zz}^{ae}/J_o^{ae} observed is due to the fact that as the level of doping grows, the FSWCNT starts flipping from nondegenerate to degenerate character (see Figure 4(a)). This is consistent with experimental data, which demonstrates that a rise in fluorine atom concentration leads to an increase in n_o, which causes the Fermi level to begin moving into the conduction band

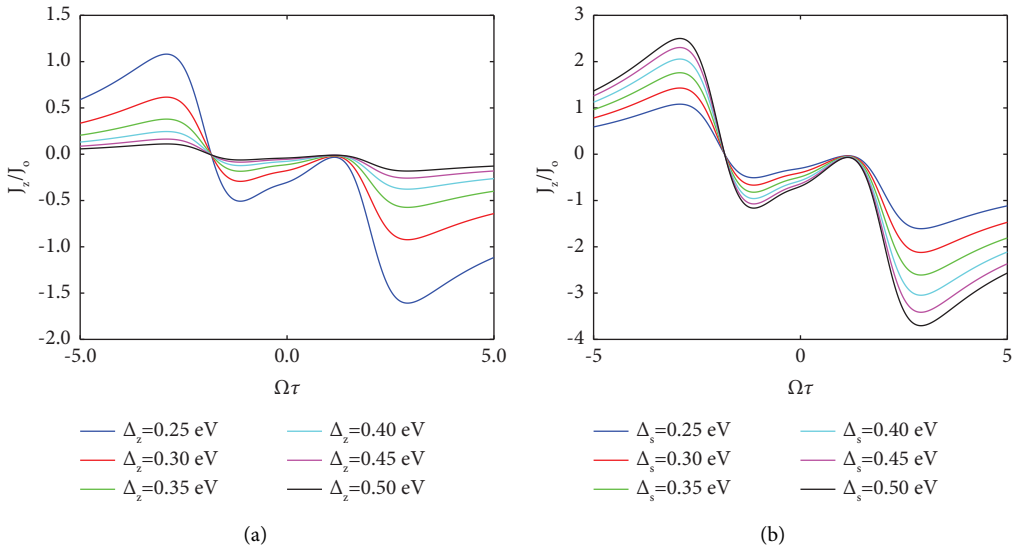

FIGURE 2: Dependence of acoustoelectric current (J_{zz}^{ae}/J_o^{ae}) on $\Omega\tau$ for different values: (a) Δ_z with $\Delta_s = 0.25$ eV, $\omega\tau = 2$, $z = 2$; (b) Δ_s with $\Delta_z = 0.25$ eV, $\omega\tau = 2$, $z = 2$.

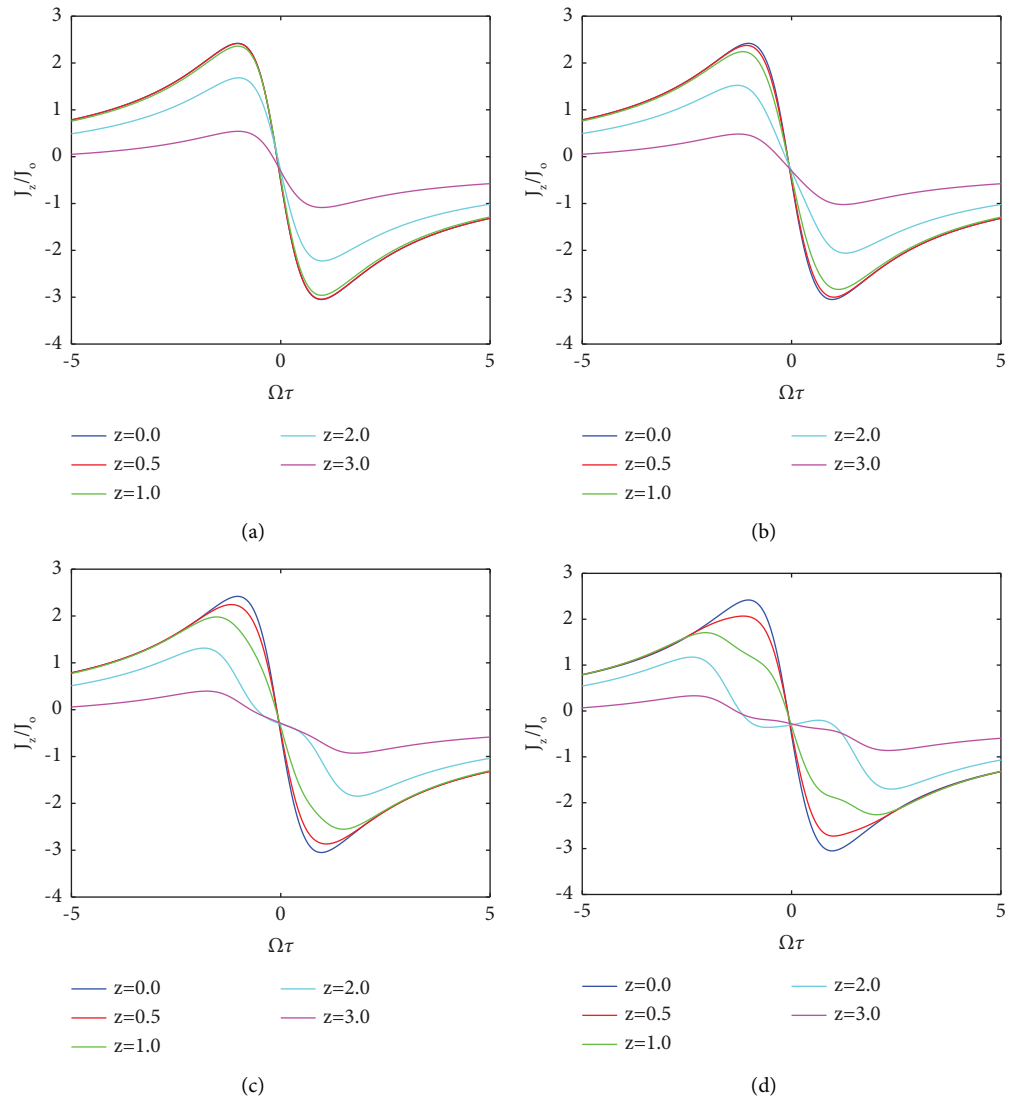

FIGURE 3: Dependence of acoustoelectric current (J_{zz}^{ae}/J_o^{ae}) on $\Omega\tau$ for different values: (a) z with $\Delta_z = 0.25$ eV, $\Delta_s = 0.25$ eV, $\omega\tau = 0$; (b) z with $\Delta_z = 0.25$ eV, $\Delta_s = 0.25$ eV, $\omega\tau = 0.5$; (c) z with $\Delta_z = 0.25$ eV, $\Delta_s = 0.25$ eV $\omega\tau = 1, z = 0$; (d) z with $\Delta_z = 0.25$ eV, $\Delta_s = 0.25$ eV, $\omega\tau = 1.5, z = 0$.

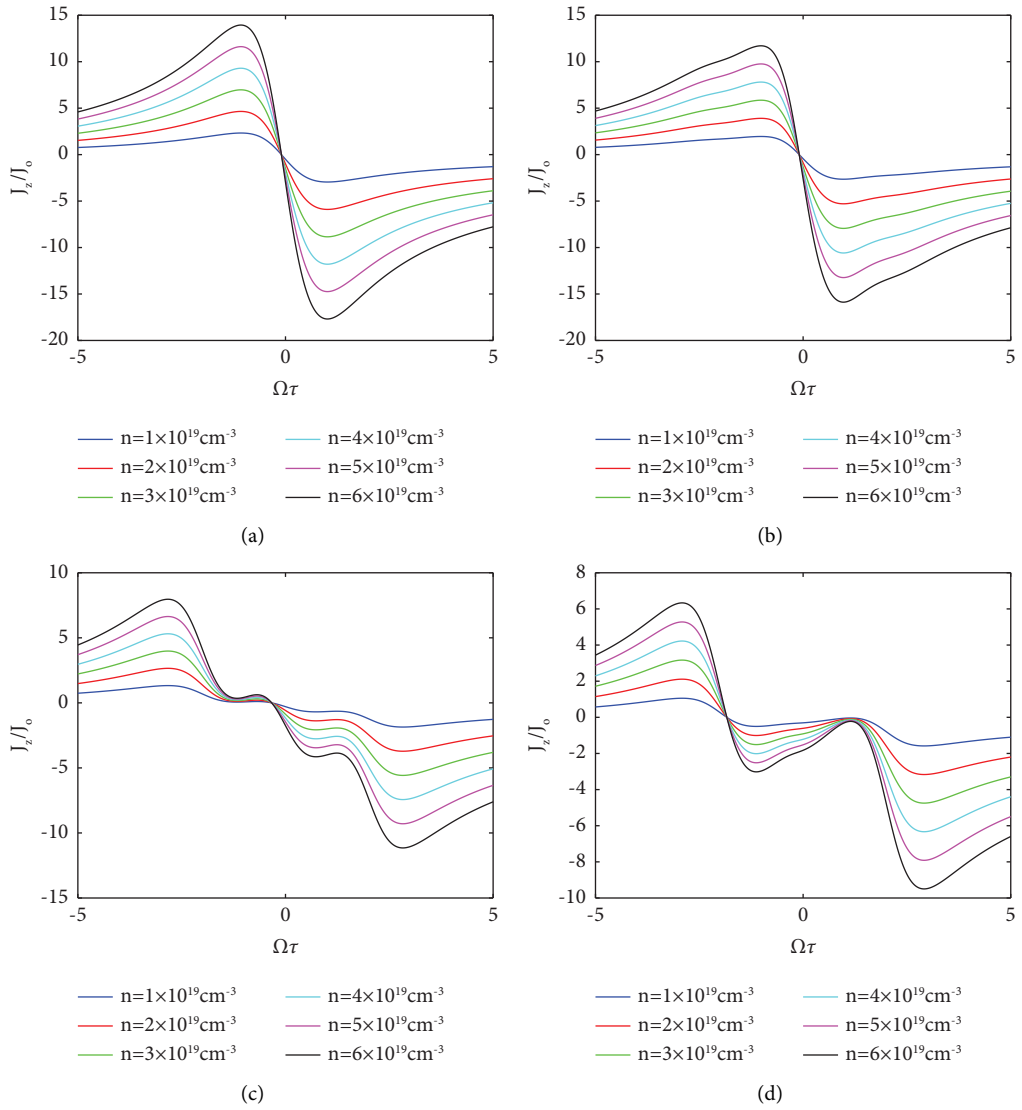

FIGURE 4: Dependence of acoustoelectric current (J_{zz}^{ae}/J_o^{ae}) on $\Omega\tau$ for different values: (a) n_o with $\Delta_s = 0.25\,\text{eV}$, $\Delta_z = 0.25\,\text{eV}$, $\omega\tau = 0.5$, $z = 0.5$; (b) n_o with $\Delta_s = 0.25\,\text{eV}$, $\Delta_z = 0.25\,\text{eV}$, $\omega\tau = 1$, $z = 2$; (c) n_o with $\Delta_s = 0.25\,\text{eV}$, $\Delta_z = 0.25\,\text{eV}$, $\omega\tau = 1.5$, $z = 2$; (d) n_o with $\Delta_s = 0.25\,\text{eV}$, $\Delta_z = 0.25\,\text{eV}$, $\omega\tau = 2$, $z = 2$.

and change the FSWCNT from nondegenerate to degenerate state. By introducing the additional carrier band structure and nonlinearly modifying the carbon $\pi-$ bonds around the Fermi level, this leads to chemical activation of the passive SWCNT surface and produces a band structure with a width of two periods. Due to fluorine's extreme electronegative nature and the $\pi-$ electrons attached to it, the SWCNT's walls weakens, which reduces the interaction of free charge carriers with the fields. The density of free carriers reduces as a result of the bonding charge change. In other words, addition of an impurity band close to the Fermi level alters the chemical potential and reduces the band gap from nondegenerate to degenerate character. Thus, there are more carriers that interact strongly with the acoustic waves to generate a high intraminiband carrier current. As $\omega\tau = 1$ and $z \gg 1$, the amplitude of the ac field starts to modulate the net current density and the carrier-phonon interaction starts to fall gradually and so as the current density (see Figure 4(b)). Moreover, when $\omega\tau = 1$ and $z \gg 1$, the peak of J_{zz}^{ae}/J_o^{ae} begins to fall, and there is an observance of a strong harmonic oscillations in this regime (see Figure 4(c)). Furthermore, in the region when $\omega\tau = 2$ and $z \gg 2$, J_{zz}^{ae}/J_o^{ae} continues to decrease further with strong harmonic oscillations observed (see Figure 4(d)).

We determined that the self-current oscillation is caused by the emergence of space charge instabilities. For a specific bias voltage in the NDV (and NDC) region, the space charge and electric field distribution in the FSWCNT is no longer uniform along the FSWCNT axis. It is predicted that there will be a space charge instability if the FSWCNT's carrier concentration (n_o) and length (L) product is sufficiently high, i.e., $nL \geq 7\epsilon\epsilon_o\mathscr{E}_c/e$, where ϵ is the dielectric constant, ϵ_o is the permittivity of free space or the electric field constant, and $\mathscr{E}_c = \hbar/ed_{s,z}\tau$ is the critical/threshold field at which

NDV (and NDC) emerges. We find that the observance of the strong space charge instability is indicative of the fact that n_oL exceeds the threshold by an order of magnitude, and thus, it is observance. However, in our FSWCNT, the NDV (and NDC) is due to Bloch oscillation miniband carriers [23]. At electric fields larger than $\mathscr{E}_c$, the carriers suffer Bragg reflection at the miniband boundary, which lead to an electric field induced localisation of carriers and consequently to a decrease of carrier velocity with increasing field [2]. At the critical field $\mathscr{E}_c$, the average mean free path of a carrier along the FSWCNT axis is given by the length $x = \Delta_{s,z}/\mathscr{E}_c$ of a trajectory, which corresponds to the path a carrier traverses when it streams from a state of minimum to a state of maximum miniband energy. At typical hypersound flux, the value of J_o at room temperature for a transistor-based single-walled carbon nanotube can be as high as $0.4mA/\mu m$ for V_{gs} of -2.5 to $-0.5V$ [50]. Moreover, this value can be high for $-0.5V$ to $5V$.

4. Conclusion

The semiclassical carrier dynamics was used to examine the axial acoustoelectric direct current (ADC) density of a nondegenerate FSWCNT under the influence of a high-frequency field in the hypersound regime. We demonstrated theoretically that the generation of THz radiation solely due to the dynamics of space charge instabilities (i.e., without resonant system) occurred due to Bragg reflection of Bloch oscillating carriers in the FSWCNT's miniband. The FSWCNT parameters n_o, Δ_s,and Δ_z, as well as $\mathscr{E}_o$ and $\mathscr{E}_1$, were found to have a significant impact on the axial ADC (J_{zz}^{ae}/J_o^{ae}). Varying (Δ_s, Δ_z, $\mathscr{E}_1$, and n_o could be used to generate and tune the FSWCNT to a high carrier drift velocity and a high fundamental frequency of the ADC self-oscillations at 300K. Interestingly, the main finding of the study was undoubtedly the proof that for a sufficiently large dc force amplitude ($\mathscr{E}_o$), ADC becomes positive over a range of negative bias ($-\mathscr{E}_o$) values, and for a range of positive bias ($+\mathscr{E}_o$), the ADC was negative. Thus, the FSWCNT can therefore function as an active device up to very high frequencies, possibly up to frequencies that correspond to the submillimeter wavelength range, and it is likely that domain suppression and acoustic Bloch gain might be obtained in purely dynamic ADC stabilisation.

Data Availability

The data that support the findings of this study are available within the article.

Additional Points

Conflicts of Interest

The authors declare that they have no conflicts of interest.

References

[1] S. A. Ktitorov, G. S. Simin, and V. Y. Sindalovskii, "American Institute of Physics," *Soviet Physics Solid State*, vol. 13, p. 1872, 1972.

[2] L. Esaki and R. Tsu, "Superlattice and negative differential conductivity in semiconductors," *IBM Journal of Research and Development*, vol. 14, no. 1, pp. 61–65, 1970.

[3] A. Wacker, "Semiconductor superlattices: a model system for nonlinear transport," *Physics Reports*, vol. 357, no. 1, pp. 1–111, 2002.

[4] M. Buttiker and H. Thomas, "Current instability and domain propagation due to Bragg scattering," *Physical Review Letters*, vol. 38, no. 2, pp. 78–80, 1977.

[5] M. Hadjazi, A. Sibille, J. F. Palmier, and F. Mollot, "Negative differential conductance in GaAs/AlAs superlattices," *Electronics Letters*, vol. 27, no. 12, pp. 1101–1103, 1991.

[6] J. F. Cadiou, J. Palmier, E. Penard et al., "Direct optical injection locking of 20 GHz superlattice oscillators," *Electronics Letters*, vol. 30, no. 20, pp. 1690-1691, 1994.

[7] J. Grenzer, A. A. Ignatov, E. Schomburg et al., "Microwave oscillator based on Bloch oscillations of electrons in a semiconductor superlattice," *Annalen der Physik*, vol. 507, no. 3, pp. 184–190, 1995.

[8] K. Hofbeck, J. Grenzer, E. Schomburg et al., "High frequency self-sustained current oscillation in an Esaki-Tsu superlattice monitored via microwave emission," *Physics Letters A*, vol. 218, no. 3-6, pp. 349–353, 1996.

[9] A. A. Ignatov, K. F. Renk, and E. P. Dodin, "Esaki-Tsu superlattice oscillator: josephson-like dynamics of carriers," *Physical Review Letters*, vol. 70, no. 13, pp. 1996–1999, 1993.

[10] H. Le Person, C. Minot, L. Boni, J. F. Palmier, and F. Mollot, "Gunn oscillations up to 20 GHz optically induced in GaAs/AlAs superlattice," *Applied Physics Letters*, vol. 60, no. 19, pp. 2397–2399, 1992.

[11] J. Kastrup, R. Klann, H. T. Grahn et al., "Self-oscillations of domains in doped GaAs-AlAs superlattices," *Physical Review B*, vol. 52, no. 19, pp. 13761–13764, 1995.

[12] B. K. Ridley, "Specific negative resistance in solids," *Proceedings of the Physical Society*, vol. 82, no. 6, pp. 954–966, 1963.

[13] P. G. Savvidis, B. Kolasa, G. Lee, and S. J. Allen, "Resonant crossover of terahertz loss to the gain of a Bloch oscillating InAs/AlSb superlattice," *Physical Review Letters*, vol. 92, no. 19, Article ID 196802, 2004.

[14] T. Hyart, K. N. Alekseev, and E. V. Thuneberg, "Bloch gain in dc-ac-driven semiconductor superlattices in the absence of electric domains," *Physical Review B*, vol. 77, no. 16, Article ID 165330, 2008.

[15] T. Hyart and K. N. Alekseev, "Nondegenerate parametric amplification in superlattices and the limits of strong and weak dissipation," *Condensed Matter Theories*, vol. 24, pp. 477–487, 2010.

[16] Y. A. Romanov, "Upwards parametric frequency conversion in superlattices," *Radiophysics and Quantum Electronics*, vol. 23, no. 5, pp. 421–428, 1980.

[17] M. W. Feise and D. S. Citrin, "Semiclassical theory of terahertz multiple-harmonic generation in semiconductor superlattices," *Applied Physics Letters*, vol. 75, no. 22, pp. 3536–3538, 1999.

[18] K. N. Alekseev, M. V. Gorkunov, N. V. Demarina, T. Hyart, N. V. Alexeeva, and A. V. Shorokhov, "Suppressed absolute negative conductance and generation of high frequency

radiation in semiconductor superlattices," *Europhysics Letters*, vol. 73, no. 6, pp. 934–940, 2006.

[19] Y. A. Romanov, J. Y. Romanova, and L. G. Mourokh, "Semiconductor superlattice in a biharmonic field: absolute negative conductivity and static electric-field generation," *Journal of Applied Physics*, vol. 99, no. 1, Article ID 013707, 2006.

[20] A. V. Shorokhov and K. N. Alekseev, "High frequency absorption and gain in superlattices: semiquasistatic approach," *Physica E: Low-Dimensional Systems and Nanostructures*, vol. 33, no. 1, pp. 284–295, 2006.

[21] S. Y. Mensah, F. K. A. Allotey, and N. G. Mensah, "Nonlinear acoustoelectric effect in a semiconductor superlattice," *Journal of Physics: Condensed Matter*, vol. 12, no. 24, pp. 5225–5232, 2000.

[22] Y. F. Ohashi, K. Kimura, and K. Sugihara, "Acousto-magnetoelectric effect in graphite," *Physica B+C*, vol. 105, no. 1-3, pp. 103–106, 1981.

[23] A. A. Ignatov, V. I. Piskarev, and V. I. Shashkin, "Instability (formation of domains) of an electric-field in multilayer quantum structures," *Soviet Physics Semiconductors-Ussr*, vol. 19, no. 12, pp. 1345–1347, 1985.

[24] A. A. Ignatov and V. I. Shashkin, "Bloch oscillations of electrons and instability of space-charge waves in superconductor superlattices," *Soviet Physics Journal of Experimental and Theoretical Physics*, vol. 66, pp. 526–530, 1987.

[25] B. Laikhtman and D. Miller, "Theory of current-voltage instabilities in superlattices," *Physical Review B*, vol. 48, no. 8, pp. 5395–5412, 1993.

[26] J. E. Baumgardner, A. A. Pesetski, J. M. Murduck, J. X. Przybysz, J. D. Adam, and H. Zhang, "Inherent linearity in carbon nanotube field-effect transistors," *Applied Physics Letters*, vol. 91, no. 5, Article ID 052107, 2007.

[27] C. Wang, A. Badmaev, A. Jooyaie et al., "Radio frequency and linearity performance of transistors using high-purity semiconducting carbon nanotubes," *ACS Nano*, vol. 5, pp. 4169–4176, 2011.

[28] M. Steiner, M. Engel, Y. M. Lin et al., "High frequency performance of scaled carbon nanotube array field-effect transistors," *Applied Physics Letters*, vol. 101, no. 5, Article ID 053123, 2012.

[29] Y. Cao, G. J. Brady, H. Gui, C. Rutherglen, M. S. Arnold, and C. Zhou, "Radio frequency transistors using aligned semiconducting carbon nanotubes with current-gain cutoff frequency and maximum oscillation frequency simultaneously greater than 70 GHz," *ACS Nano*, vol. 10, no. 7, pp. 6782–6790, 2016.

[30] D. Zhong, Z. Zhang, L. Ding et al., "Gigahertz integrated circuits based on carbon nanotube films," *Nat. Electronic*, vol. 1, pp. 40–45, 2017.

[31] S.-J. Han, J. Tang, B. Kumar et al., "High-speed logic integrated circuits with solution-processed self-assembled carbon nanotubes," *Nature Nanotechnology*, vol. 12, no. 9, pp. 861–865, 2017.

[32] L. Liu, L. Ding, D. Zhong et al., "Carbon nanotube complementary gigahertz integrated circuits and their applications on wireless sensor interface systems," *ACS Nano*, vol. 13, no. 2, pp. 2526–2535, 2019.

[33] C. Kocabas, H.-S. Kim, T. Banks et al., "Radio frequency analog electronics based on carbon nanotube transistors," *Proceedings of the National Academy of Sciences of the United States of America*, vol. 105, no. 5, pp. 1405–1409, 2008.

[34] P. Taborowska, G. Stando, M. Sahlman, M. Krzywiecki, M. Lundström, and D. Janas, "Doping of carbon nanotubes by halogenated solvents," *Scientific Reports*, vol. 12, no. 1, pp. 7004–7010, 2022.

[35] B. Kumanek, T. Wasiak, G. Stando, P. Stando, D. Łukowiec, and D. Janas, "Simple method to improve electrical conductivity of films made from single-walled carbon nanotubes," *Nanomaterials*, vol. 9, no. 8, p. 1113, 2019.

[36] B. Kumanek, G. Stando, P. Stando et al., "Enhancing thermoelectric properties of single-walled carbon nanotubes using halide compounds at room temperature and above," *Scientific Reports*, vol. 11, no. 1, pp. 8649–8718, 2021.

[37] J. L. Blackburn, A. J. Ferguson, C. Cho, and J. C. Grunlan, "Carbon-nanotube-based thermoelectric materials and devices," *Advanced Materials*, vol. 30, no. 11, Article ID 1704386, 2018.

[38] J. Ravichandran, "Thermoelectric and thermal transport properties of complex oxide thin films, heterostructures and superlattices," *Journal of Materials Research*, vol. 32, no. 1, pp. 183–203, 2017.

[39] K. Seeger, "High-frequency-induced phase-dependent dc current by Bloch oscillator non-ohmicity," *Applied Physics Letters*, vol. 76, no. 1, pp. 82–84, 2000.

[40] S. S. Abukari, K. W. Adu, S. Y. Mensah et al., "Rectification due to harmonic mixing of two coherent electromagnetic waves with commensurate frequencies in carbon nanotubes," *The European Physical Journal B*, vol. 86, no. 3, pp. 106–114, 2013.

[41] S. Mensah, G. M. Shmelev, and M. Pshten, "Izvestiya vysshikh uchebnykh zavedenii, fizika," *Translated in Russian Phys. Journal*, vol. 6, p. 112, 1988.

[42] D. Sakyi-Arthur, S. Y. Mensah, N. G. Mensah, K. A. Dompreh, and R. Edziah, "Absorption of acoustic phonons in fluorinated carbon nanotube with non-parabolic, double periodic band," *Phonons in Low Dimensional Structures*, InTech, pp. 129–142, New York, NY, USA, 2018.

[43] D. Sakyi-Arthur, S. Y. Mensah, K. W. Adu et al., "Induced Hall-like current by acoustic phonons in semiconductor fluorinated carbon nanotube," *World Journal of Condensed Matter Physics*, vol. 10, no. 2, pp. 71–87, 2020.

[44] D. Sakyi-Arthur, S. Y. Mensah, K. W. Adu, K. A. Dompreh, R. Edziah, and N. G. Mensah, "Acoustoelectric effect in fluorinated carbon nanotube in the absence of external electric field," *World Journal of Condensed Matter Physics*, vol. 10, no. 01, pp. 1–11, 2020.

[45] D. Sakyi-Arthur, S. Y. Mensah, K. W. Adu et al., "Semiconductor fluorinated carbon nanotube as a low voltage current amplifier acoustic device," *World Journal of Condensed Matter Physics*, vol. 10, no. 1, pp. 12–25, 2020.

[46] D. Sakyi-Arthur, S. Y. Mensah, N. G. Mensah, K. W. Adu, K. A. Dompreh, and R. Edziah, "Tunable power factor in fluorine-doped single-walled carbon nanotubes," *Journal of Applied Physics*, vol. 128, no. 24, Article ID 244301, 2020.

[47] D. Sekyi-Arthur, M. Egblewogbe, S. Y. Mensah et al., "Giant thermoelectric figure of merit in fluorine-doped single walled-carbon nanotubes," *Physica E: Low-Dimensional Systems and Nanostructures*, vol. 142, Article ID 115292, 2022.

[48] N. R. Sadykov, E. Y. Kocherga, and P. N. D'yachkov, "Nonlinear current in modified nanotubes with exposure to alternating and constant electric fields," *Russian Journal of Inorganic Chemistry*, vol. 58, no. 8, pp. 951–955, 2013.

[49] D. Sekyi-Arthur, S. Y. Mensah, K. A. Dompreh, G. Nkrumah-Buandoh, and N. G. Mensah, "Giant thermoelectric power in fluorine-doped single-walled carbon nanotubes," *Journal of Physics and Chemistry of Solids*, vol. 171, Article ID 111020, 2022.

[50] D. Sekyi-Arthur, S. Y. Mensah, E. K. Amewode, C. Jebuni-Adanu, and J. Asare, "High frequency amplification of acoustic phonons in fluorine-doped single-walled carbon nanotubes," *Diamond and Related Materials*, vol. 141, Article ID 110642, 2024.

[51] D. A. Romanov and O. V. Kibis, "Magnetocontrolled quantum states in helicoidal tubules," *Physics Letters A*, vol. 178, no. 3-4, pp. 335–337, 1993.

[52] D. Sekyi-Arthur, S. Y. Mensah, E. Amewode, R. Arthur, and R. R. Adams, "Acoustoelectric direct current density in fluorine doped single-walled carbon nanotubes due to harmonic mixing of bichromatic fields with commensurate frequencies," *Diamond and Related Materials*, vol. 136, Article ID 109993, 2023.

[53] O. M. Yevtushenko, G. Y. Slepyan, S. A. Maksimenko, A. Lakhtakia, and D. A. Romanov, "Nonlinear electron transport effects in a chiral carbon nanotube," *Physical Review Letters*, vol. 79, no. 6, pp. 1102–1105, 1997.

[54] G. Y. Slepyan, S. A. Maksimenko, A. Lakhtakia, O. M. Yevtushenko, and A. V. Gusakov, "Electronic and electromagnetic properties of nanotubes," *Physical Review B*, vol. 57, no. 16, pp. 9485–9497, 1998.

[55] G. Y. Slepyan, S. A. Maksimenko, A. Lakhtakia, O. Yevtushenko, and A. V. Gusakov, "Electrodynamics of carbon nanotubes: dynamic conductivity, impedance boundary conditions, and surface wave propagation," *Physical Review B*, vol. 60, no. 24, pp. 17136–17149, 1999.

[56] Y. Miyamoto, S. G. Louie, and M. L. Cohen, "Chiral conductivities of nanotubes," *Physical Review Letters*, vol. 76, no. 12, pp. 2121–2124, 1996.

[57] S. Y. Mensah, F. K. A. Allotey, and S. K. Adjepong, "The effect of a high frequency electric field on hypersound amplification in a superlattice," *Journal of Physics: Condensed Matter*, vol. 6, pp. 3479–3485, 1994.